

Amplification of Seismic Waves by the Seattle Basin, Washington State

by Thomas L. Pratt, Thomas M. Brocher, Craig S. Weaver, Kenneth C. Creager, Catherine M. Snelson,* Robert S. Crosson, Kate C. Miller, and Anne M. Tréhu

Abstract Recordings of the 1999 M_w 7.6 Chi-Chi (Taiwan) earthquake, two local earthquakes, and five blasts show seismic-wave amplification over a large sedimentary basin in the U.S. Pacific Northwest. For weak ground motions from the Chi-Chi earthquake, the Seattle basin amplified 0.2- to 0.8-Hz waves by factors of 8 to 16 relative to bedrock sites west of the basin. The amplification and peak frequency change during the Chi-Chi coda: the initial *S*-wave arrivals (0–30 sec) had maximum amplifications of 12 at 0.5–0.8 Hz, whereas later arrivals (35–65 sec) reached amplifications of 16 at 0.3–0.5 Hz. Analysis of local events in the 1.0- to 10.0-Hz frequency range show fourfold amplifications for 1.0-Hz weak ground motion over the Seattle basin. Amplifications decrease as frequencies increase above 1.0 Hz, with frequencies above 7 Hz showing lower amplitudes over the basin than at bedrock sites. Modeling shows that resonance in low-impedance deposits forming the upper 550 m of the basin beneath our profile could cause most of the observed amplification, and the larger amplification at later arrival times suggests surface waves also play a substantial role. These results emphasize the importance of shallow deposits in determining ground motions over large basins.

Introduction

When a large earthquake like those discerned from paleoseismic and geologic evidence eventually strikes the Pacific Northwest (Atwater, 1996; Bucknam *et al.*, 1992), the sedimentary basins in the area likely will amplify ground shaking, as they do in other areas (e.g., Liu and Heaton, 1984; Frankel, 1994; Wald and Graves, 1998; Sánchez-Sesma *et al.*, 1988, 1993). Understanding the magnitude of this amplification, and the frequency at which it occurs, is crucial to building structures on basin sediments. The 70- by 25-km Seattle basin (Johnson *et al.*, 1994; Pratt *et al.*, 1997; Brocher *et al.*, 2001a) is of particular concern because it underlies some of the largest cities in the Cascadia region (Seattle, Kirkland, Bellevue, and Redmond, Washington). Observational data for determining site response over the Seattle basin has been limited by the small number of instruments deployed over only a portion of the basin (Carver *et al.*, 1998; Frankel *et al.*, 1999; Hartzell *et al.*, 2000; Frankel *et al.*, 2002). Estimates of the basin response to seismic waves therefore rely in a large part on forward modeling using relatively simple models (Langston and Lee, 1983; Ihnen and Hadley, 1986; Frankel and Stephenson, 2000; Hartzell *et al.*, 2002).

A unique opportunity to directly measure the response of the Seattle basin to seismic waves occurred in 1999, when

we recorded arrivals from the M_w 7.6 Chi-Chi, Taiwan, earthquake (Shin *et al.*, 2000) on 29 seismometers deployed across the basin for a seismic refraction survey (Fig. 1) (Brocher *et al.*, 2000a, b; Snelson *et al.*, 2000). Shear waves from the Chi-Chi earthquake were well recorded in the 0.1- to 1-Hz frequency range (10- to 1-sec periods), and these waves showed substantially larger amplitudes over the Seattle basin than at bedrock sites at the ends of the array (Figs. 2–3a). To supplement these observations of low-frequency waves, we examined ground motions at 1.0–10 Hz on the same instruments from two local earthquakes and five of our largest refraction blasts. Although both of these data sets have shortcomings because the seismometer array was not designed for a site response study, they provide a unique set of data for looking at seismic-wave amplification. In this article we document the characteristics of these weak ground motions over the Seattle basin, and we discuss the likely causes of this amplification.

Observations

In 1999, the second of the Seismic Hazard Investigations of Puget Sound (SHIPS), a crustal reflection and refraction experiment, was undertaken to image the 7.5- to 10-km thickness of Eocene to Holocene sedimentary strata filling the Seattle basin (Brocher *et al.*, 2000a, b; Snelson *et al.*, 2000). The 1999 SHIPS experiment used 1008 seismom-

*Present address: Department of Geosciences, University of Nevada, Las Vegas, 4505 Markland Parkway, Las Vegas, Nevada 89154-4010.

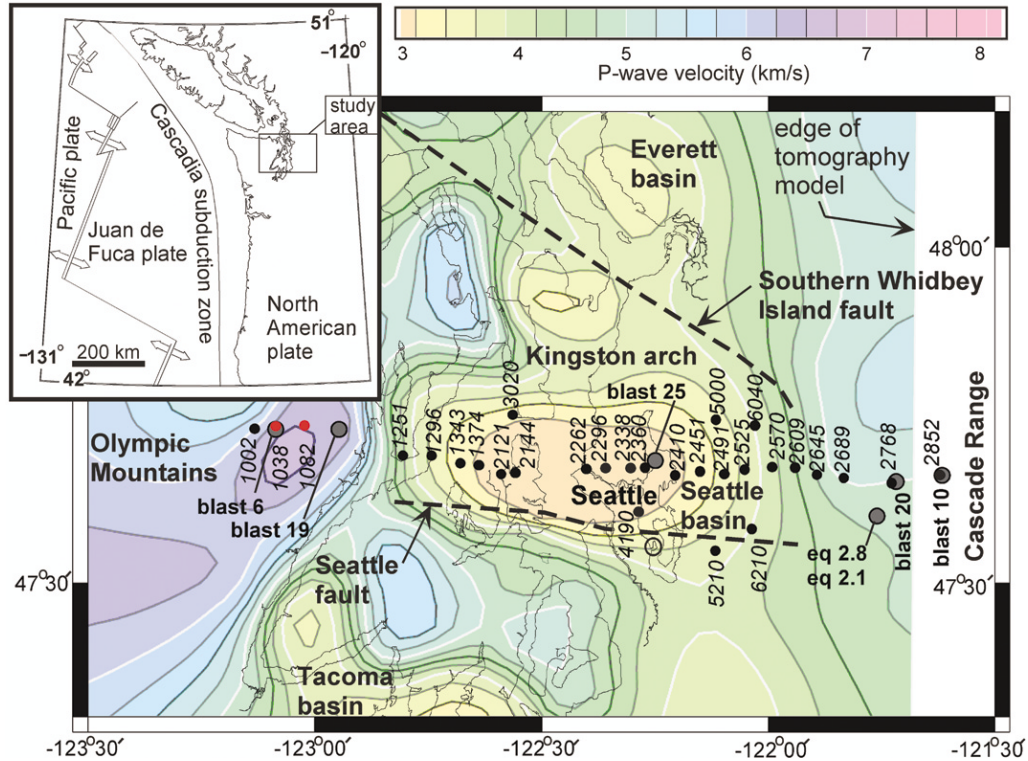


Figure 1. Map of the 1999 Seismic Hazard Investigations in Puget Sound (SHIPS) experiment. Black and red dots denote continuously recording seismograph stations, and red dots denote the two stations we used as reference sites. Gray dots denote local earthquakes (magnitudes listed) and blasts. Dashed lines show major faults (Pratt *et al.*, 1997; Brocher *et al.*, 2001a). The colored background is a P -wave tomographic image at 2.5-km depth (Van Wagoner *et al.*, 2002), on which the Seattle basin appears as an area of low velocity. Stations 1002–1082 and 2768–2852 are on bedrock, stations 5210 and 6210 are in the Seattle fault zone, and other stations are located above the basin. The open circle shows the location of the Seward Park reference site used in previous site response studies of the Seattle area (Frankel *et al.*, 1999; Hartzell *et al.*, 2000; Frankel *et al.*, 2002).

eters deployed in an east–west line across the center of the Seattle basin and in four short north–south arrays. Most of these seismometers were single-component instruments programmed to record short time windows coinciding with our blasts, but 29 three-component seismometers dispersed through the array were programmed to record continuous data throughout the 4 days of the experiment. We obtained data from 23 of these seismometers sited along the main east–west profile and 6 seismometers along the cross profiles (Fig. 1). Instruments consisted of identical Reftek data loggers and 4.5-Hz, L-28 geophones whose horizontal axes were oriented to magnetic north and east (about 20° east of true north). A 4-msec sample rate was used for the recordings. The data are available as part of a CD-ROM collection of waveforms from the Chi-Chi event (Brocher *et al.*, 2001b).

Strong arrivals from the Chi-Chi, Taiwan, earthquake of 21 September 1999 were recorded on 28 of the SHIPS three-component seismometers (Fig. 2; station 2262 malfunctioned). The Chi-Chi earthquake was located 89° from the Puget Lowland at a backazimuth of 305° , resulting in an

incidence angle of about 16° for arrivals entering the bottom of the Seattle basin. Because the geophones were oriented at about a 20° azimuth (to magnetic north), the north–south component is nearly tangential and the east–west component is nearly radial to the incident waves.

In spite of the 4.5-Hz geophone frequency, the S -wave arrivals from the Chi-Chi earthquake showed a strong signal between 0.1 and 0.7 Hz at many of the SHIPS stations (Figs. 2, 3a, and 4). The continuity of the arrivals (Figs. 2–3) and the consistency of the amplitudes across the array (discussed subsequently) indicate the recorded amplitudes are reliable, even though the frequencies are at the lower end of the geophone response curve. The signal-to-noise ratio at most stations reaches 4, although noise levels progressively increase with frequency until they approach the signal strength near 1 Hz at many stations (Fig. 4). The aftershocks to the Chi-Chi event reached M_w 6.5 and showed clear P -wave arrivals on our array, but S -wave arrivals from the aftershocks were too weak to use in our analysis. No other teleseisms produced strong arrivals on the array.

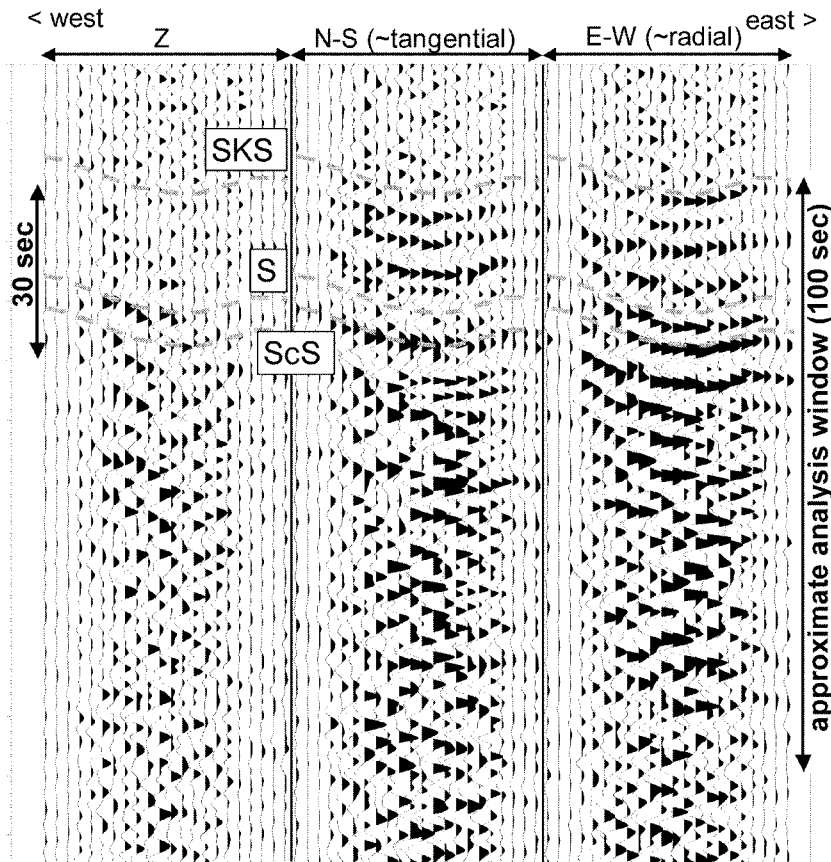


Figure 2. *S*-wave arrivals from the 1999 M_w 7.6 Chi-Chi, Taiwan, earthquake recorded on the main east–west line of the SHIPS seismic array. Traces, which are scaled equally, are arranged in three panels with vertical components on the left, north–south components in the center, and east–west components on the right. Within each panel, the traces are arranged from west (left) to east (right). The vertical axis is time in seconds (each tick is 10.0 sec). The first clear *S*-wave arrival (*SKS*) is marked by the gray dashed line, whose shape is determined by the nonvertical incidence angle and the low-velocity sediments of the Seattle basin. The *S* and *ScS* phases arrive 19 and 24 sec after the initial *SKS* arrival. Note that the amplitudes are largest in the center of the array and are smaller at the bedrock sites at both ends of the array. The initial *S*-wave arrivals are barely visible on the vertical component, but are prominent on the horizontal components. Phases beginning 20–30 sec after the initial arrival are interpreted to contain surface waves and scattered energy because they are visible on the vertical component and are incoherent across the array. Data have a 0.05–0.1–0.35–0.7 Hz, trapezoidal bandpass filter.

S waves from the Chi-Chi earthquake show substantially larger amplitudes and longer durations on instruments sited over the Seattle basin than at adjacent bedrock sites in the Olympic Mountains and Cascade Range (Figs. 2–3a). The initial *S*-wave arrival is the *SKS* phase, which, in an isotropic, spherically symmetric earth should appear only on the radial component. The *SKS* arrivals are followed 19 and 24 sec later by the *S* and *ScS* phases. The early *S*-wave arrivals, dominated by these direct phases incident from below, are coherent across the entire array and are weak on the vertical component (Fig. 2). Later arrivals, 30–100 sec after the *SKS* arrival, are less coherent between stations and are evident on the vertical component. The incoherent nature and the vertical motion of these later arrivals are consistent with the presence of basin surface waves and other scattered energy of local origin beginning about 20 sec after the initial *S*-wave arrivals and becoming the dominant phases after about 40 sec.

To supplement the low-frequency information from the Chi-Chi earthquake, we analyzed arrivals in the 1- to 10-Hz frequency range from two local earthquakes and five blasts. Although a subset of our three-component seismometers recorded 26 local earthquakes and quarry blasts, only 2 local events had clear arrivals at all of our stations (e.g., Fig. 3b). These earthquakes were coda magnitude 2.8 and 2.1 events with identical epicenters near the east end of the array, with focal depths of 16.9 and 15.9 km, respectively (Fig. 1)

(Brocher *et al.*, 2000b). We also analyzed records from five of our largest refraction blasts (Fig. 1): two from the east end of the array (blasts 10 and 20; 1091 and 909 kg of explosive, respectively), two from the west end of the array (blasts 6 and 19; 1273 and 909 kg of explosive, respectively), and the largest blast from near the center of the array (blast 25; 182 kg of explosive). These blasts emitted smaller amounts of *S*-wave energy and had lower signal-to-noise ratios than the earthquakes, especially in the urbanized area in the east-central part of the array (e.g., Fig. 3c), but the *S*-wave arrivals were nonetheless evident as increased amplitudes at most of the stations. The spectral ratios computed from the five blasts were similar to those from the two local earthquakes (Fig. 4). Despite the potential shortcomings of using the blasts, we felt that the additional source azimuths merited their inclusion in the analysis.

The combination of the Chi-Chi arrivals and the local events provides a complete frequency spectrum from 0.1 to 10 Hz for our analysis. However, the 0.7- to 1.0-Hz portion of the Chi-Chi spectrum and the 1.0- to 2.0-Hz portion of the spectrum from the local events have high noise levels. The 0.7- to 2.0-Hz portion of the spectral ratios should therefore be interpreted with caution.

Analysis

To quantify the amplification across the 1999 SHIPS array, we computed spectral ratios of the arrivals from the Chi-

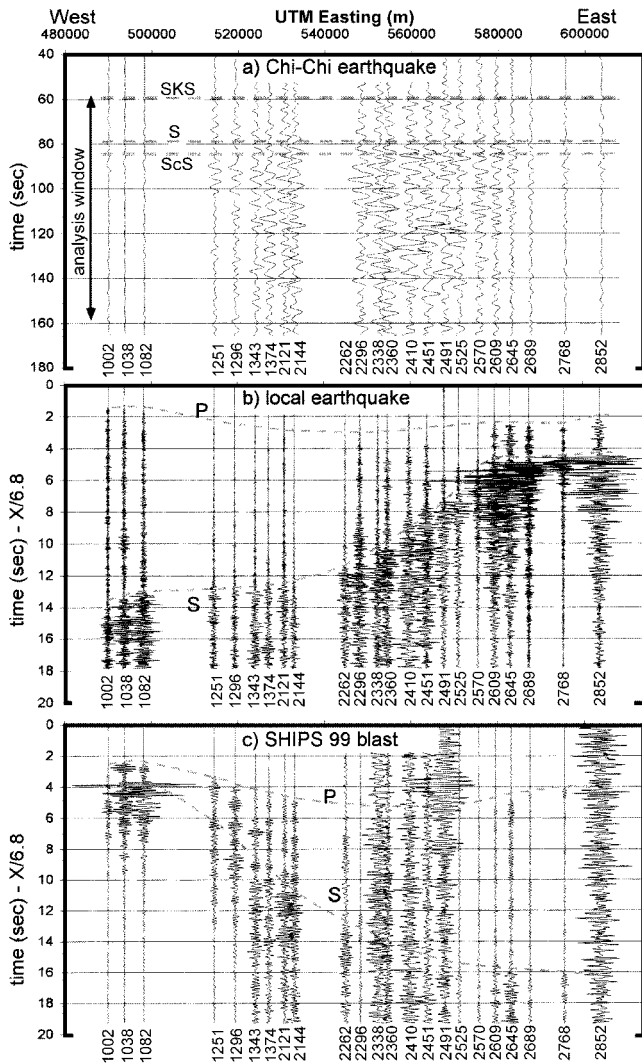


Figure 3. Records of earthquakes and blasts recorded on the east-west component of the 1999 SHIPS receiver array. (a) *S*-wave arrivals (*SKS*, *S*, *ScS*) from the Chi-Chi earthquake. Large amplitudes and long durations of shaking are evident over the Seattle basin. Data have a 0.05–0.1–0.35–0.7 Hz, trapezoidal bandpass filter. Time 0 is arbitrary. (b) Recordings from an *M* 2.8 earthquake located about 17 km beneath the east end of the array. Note the strong *S*-wave arrivals. Traces have a spherical spreading correction ($1/\text{radius}$) and a 0.1–0.4–10–20 Hz, trapezoidal bandpass filter. Time 0 is the origin time of the earthquake. (c) Recordings of the SHIPS 99 blast 19 near the west end of the array. The *P*- and *S*-wave arrivals are apparent at most stations, but are obscured by noise in the Seattle and Redmond urban area (stations 2338–2491) and at station 2852. Data have a spherical spreading correction ($1/\text{radius}$) and a 0.1–0.4–5–10 Hz, trapezoidal bandpass filter. The detonation of the blast was set at 2.0 sec.

Chi earthquake relative to the average of two bedrock sites in the Olympic Mountains at the west end of the array (stations 1038 and 1082; Figs. 1 and 4). All data were first corrected for amplitude shifts (steps) caused by voltage drops when the disk drives in the recorders turned on and off. The times of disk-drive activity were determined from the seismometer log files, and the amplitude of the step was measured on the traces after applying a low-pass filter. We then aligned the *S*-wave arrivals to remove time delays introduced by the basin sediments and the nonvertical incidence angle (dashed line in Fig. 2). These static corrections were made by picking the arrival times for a prominent, impulsive *P*-wave arrival recorded on the vertical components, then multiplying the time differences by 1.8 to get an approximate *S*-wave static correction. Amplitude spectra were taken in a 100-sec time window beginning at the first obvious *S*-wave arrival (Fig. 2), and the vector sum (square, sum, square root) of the two horizontal-component spectra were computed and smoothed with a tapered 0.15-Hz running average.

We divided each site's spectrum by the average of the two reference sites to obtain a spectral ratio at each station (Fig. 4). Bedrock (Eocene Crescent Formation volcanic rock) is exposed throughout the area surrounding these reference sites, although the seismometers themselves are located in soil over the bedrock. The geology beneath the reference sites consists of a thick sequence of Eocene volcanic and sedimentary rocks (Crescent Formation) overlying the accretionary prism sediments and subducted oceanic plate.

To estimate the signal-to-noise ratio of the Chi-Chi recordings, we took the amplitude spectra in a 100-sec time window before the *P*-wave arrival from the Chi-Chi earthquake and processed these noise traces in an identical manner and using the same reference signal as our data. Results are plotted on the same graphs as the spectral ratios from the *S*-wave arrivals (Fig. 4). Although in most cases the noise levels appear to be characteristic of the site, station 2852 showed intermittent high noise levels at frequencies near 1.0 Hz (e.g., Fig. 3c) that were not present in the noise window (Fig. 4). At most stations the signal-to-noise ratio exceeds 4 for at least part of the spectrum, but decreases to 2 or lower near 0.1 Hz and near 1.0 Hz (Fig. 4).

The signal-to-noise ratio is a concern at the reference sites, but we do not see a better alternative for a reference signal. Noise levels at the reference sites were the lowest of any sites in the array (Fig. 4), but the signal from the Chi-Chi event was also much smaller than the amplified signals characterizing the basin sites (Fig. 3a). Normalized plots of traces from the reference stations show waveforms that are similar to each other and, during the main *S*-wave arrivals, similar in shape to traces at nearby basin sites (Fig. 5a). This similarity of waveforms indicates the reference sites are indeed recording the *S*-wave arrivals, but with a lower signal strength than at the basin sites. Plots of the raw spectral amplitudes show that the reference sites have a relatively flat response in comparison to the response at instruments situated on even a small thickness of basin sediment (Fig. 5b).

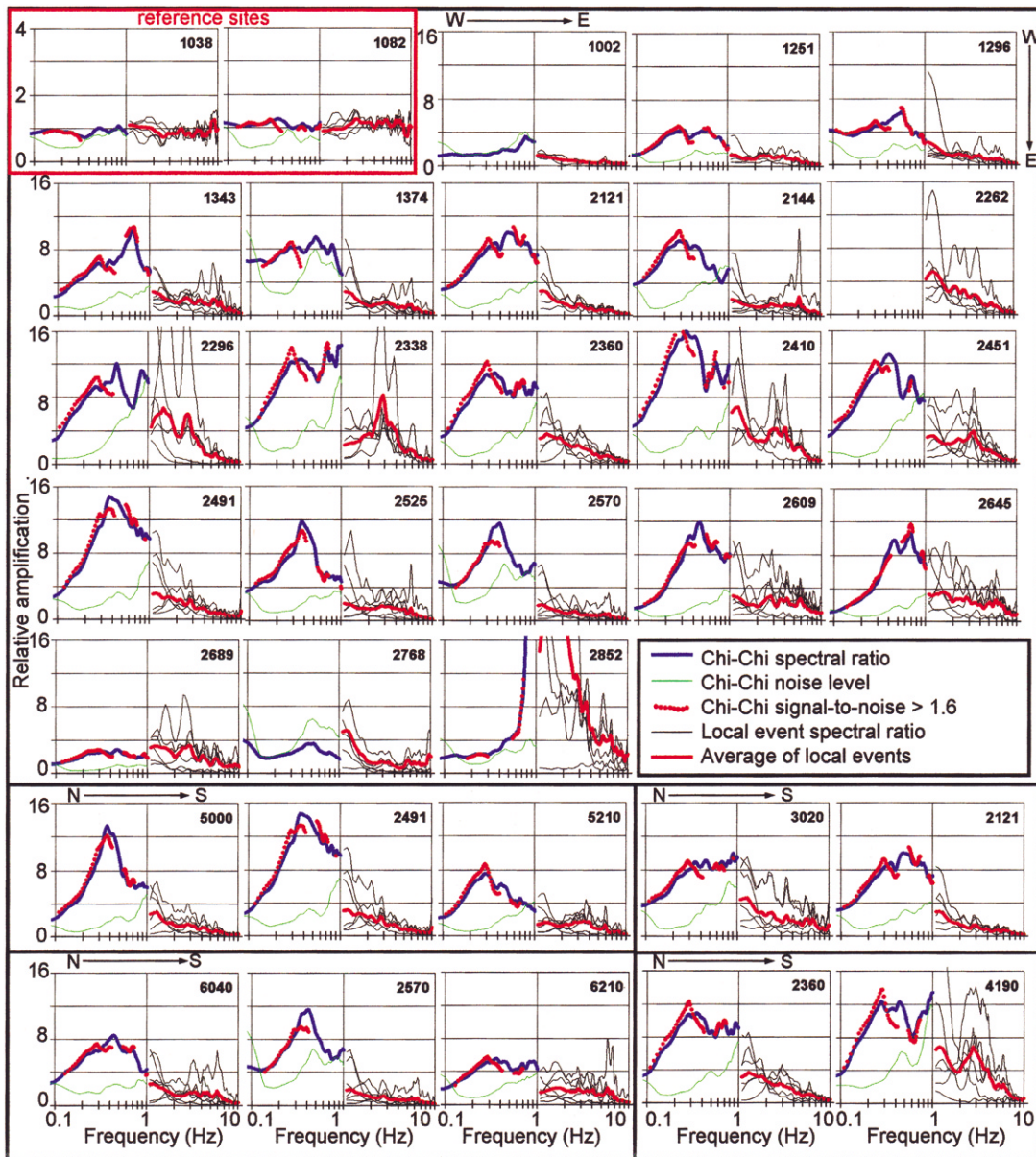


Figure 4. Graphs showing the spectral amplitudes at our instrument sites relative to the average of bedrock sites 1038 and 1082. Graphs are arranged from west (top left) to east (bottom right) for stations 1002–2768. In the bottom two rows, the graphs are arranged as two- or three-station north–south arrays (Fig. 1). Within each graph, the response of the station to the Chi-Chi event is shown at low frequencies (0.1–1 Hz), with the heavy blue line being the response and the light green line being the noise level in a 100-sec window just before the *P*-wave arrival (but divided by the same reference spectrum as the signal). The red dots below 1.0 Hz are the response where the signal-to-noise ratio is greater than 1.6 and the noise spectra has been subtracted from the observed spectra. Above 1.0 Hz are thin black lines representing the response to the individual blasts and local earthquakes, with the heavy red line being the average to these seven local events. The portions of the spectra between 0.7 and 2.0 Hz are suspect because of high noise levels (see text). Station 2852 has high noise levels between 0.7 and 4.0 Hz (Fig. 3c).

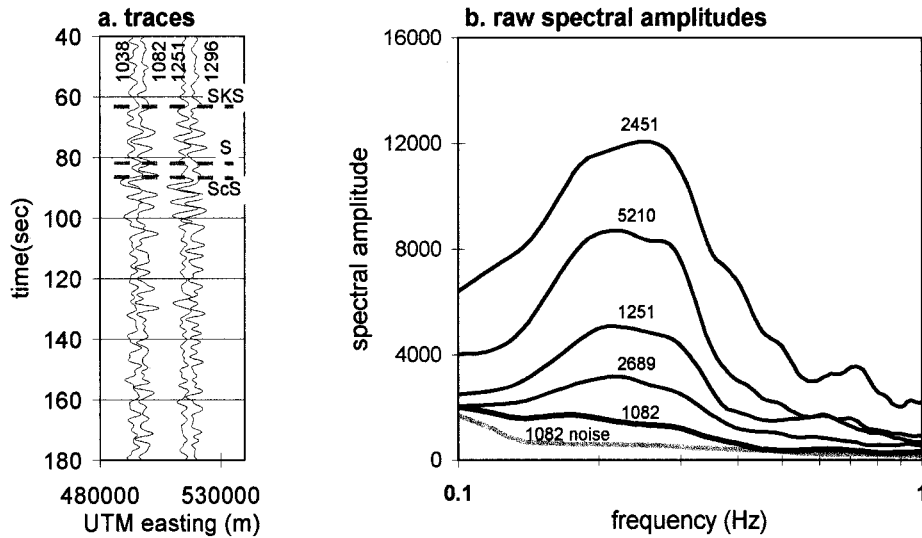


Figure 5. Traces at the reference sites compared with two adjacent sites, and raw spectral amplitudes of the Chi-Chi arrivals. (a) The two reference sites are in phase and similar to the adjacent sites, indicating they are recording signal. Traces are scaled to have the same peak amplitudes and have a 0.05-0.1-0.35-0.7 Hz bandpass filter. (b) Raw spectral amplitudes of the Chi-Chi arrivals in a 100-sec time window beginning just before the *S*-wave arrivals. Note the relatively flat response at the reference site (1082) compared with stations on the basin. The spectral amplitude at station 1082 is near noise levels above 0.4 Hz. Other sites are from the edges of the Seattle basin (stations 2689, 1251, and 5210) and from the center of the basin (2451).

The noise levels at the reference sites are also low, but nonetheless are nearly equal to the signal level at frequencies above 0.4 Hz (Figs. 4 and 5b). All sites with a better signal-to-noise ratio than our reference sites were basin sites that show much larger amplitudes in the raw spectra, indicating amplification from basin effects (Fig. 5b). We therefore prefer to use the Olympic Mountain bedrock sites as the reference signal, rather than using basin sites that clearly showed amplification.

To estimate the portions of the spectra that have a signal-to-noise ratio high enough to be reliable, we recomputed the spectral ratios only where the signal-to-noise levels at both the site and at least one reference site were both greater than 1.6. For the portions of the spectra with an appropriate signal-to-noise ratio, we subtracted the noise spectrum from the observed spectrum (root mean square difference), under the assumption that this difference approximates the true signal level. If both of the reference sites had an appropriate signal-to-noise ratio, we used the average. If only one of the reference sites had an appropriate signal-to-noise level, we used only one of the reference sites, and we did not compute a spectral ratio if both of the reference sites were unsuitable. The result, plotted in red below 1.0 Hz in Figure 4, is a spectral ratio that covers only the part of the spectrum with a reasonably good signal-to-noise ratio. Note in Figure 4 that sites 1002 and 2768 had signal levels too low for computation, that neither of the reference sites have a good signal-to-noise ratio over the entire spectrum, and that many sites have little or no spectral ratio computed at frequencies above

0.4 Hz. Where the signal-to-noise ratio was high enough, these recomputed spectra were in close agreement with the simple spectral ratios computed earlier.

To analyze the local events and blasts, we first reduced the records using a velocity of 3.5 km/sec to approximately align the *S*-wave arrivals across the array. We then computed the amplitude spectra of the horizontal component records in a 10-sec time window beginning at the predicted arrival time of the *S* wave. After taking the vector sum of the two horizontal components, we corrected the amplitudes for simple spherical spreading ($1/\text{radius}$) and attenuation ($e^{-\pi f t/Q}$, f = frequency, t = travel time, Q = attenuation factor). For the attenuation factor (Q), we used the relation $Q = 380f^{0.39}$ derived from regional studies (Atkinson, 1995) and used in previous site response studies in the Seattle area (Frankel *et al.*, 1999; Hartzell *et al.*, 2000). Records from receivers within 14 km of the blasts were omitted because the signal at receivers near the source was of short duration and extremely high amplitude (e.g., Fig. 3c). We also removed traces that were contaminated by exceptionally high noise levels. Dividing each site spectrum by the average of our two reference sites gave us the final spectral ratios for each event at each site (Fig. 4). We averaged the response from the two local earthquakes and five blasts to produce an average spectral ratio function for each station (red line above 1.0 Hz in Fig. 4).

Results are presented as graphs of the individual spectra (Fig. 4) and as profiles over the Seattle basin at specific frequencies (Fig. 6). Below 1.0 Hz, the individual spectra

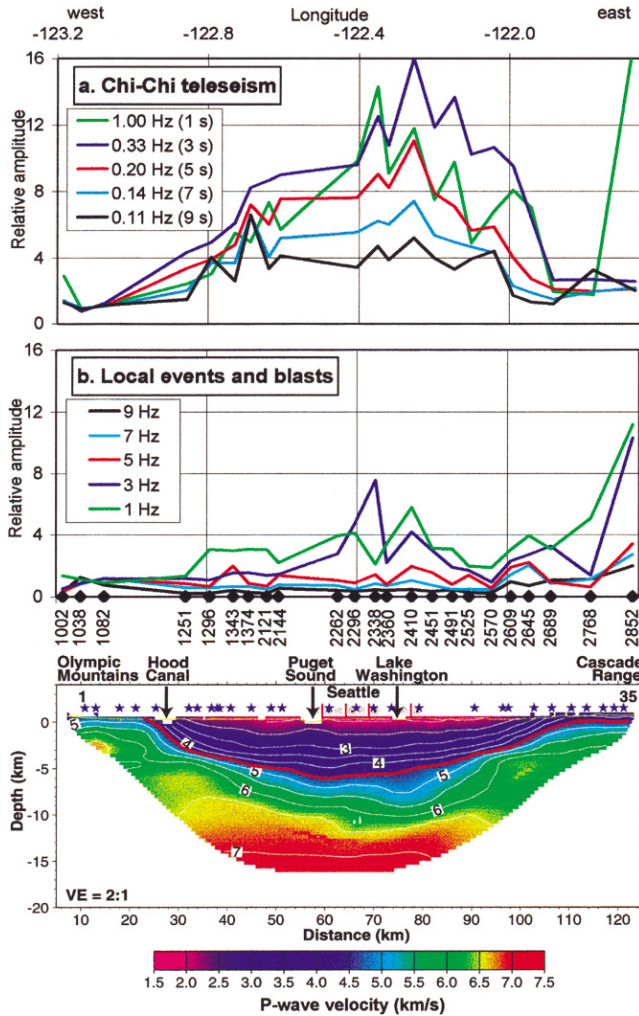


Figure 6. Profiles across the Seattle basin showing spectral amplitudes at specific frequencies relative to bedrock sites (a, b) and a profile showing the P -wave velocity structure of the Seattle basin derived from tomographic analysis of the 1999 SHIPS data (bottom). The numbers in parentheses in the legend on the top graph are the wave periods in seconds. The red contour on the velocity model (4.5 km/sec) is interpreted to be near the top of basement rocks below the basin. Note the large amplification of 1.0- to 0.2-Hz waves (1- to 5-sec periods) over the basin (a). Stations contributing to the upper plots are listed, as are the locations of the Olympic Mountains, the Cascade Range, the city of Seattle, and our blasts (stars).

show the amplification of the Chi-Chi earthquake arrivals, as well as the noise level at each of the stations. Above 1.0 Hz, the graphs show the amplification of the two local earthquakes and five blasts, plus the average of these events. The profiles (Fig. 6) show only the average amplitudes at the selected frequencies.

The variation in amplitude between adjacent stations (Fig. 6) provides an estimate of the reliability of the long-period amplitudes (1–10 sec) on these relatively high-frequency seismometers (4.5 Hz). The amplitudes of specific

frequencies vary by about 30% between adjacent stations across most of the profiles (Fig. 6). This variation could be due entirely to differences in the site responses at the sites, but we cannot eliminate the possibility that at least part of the variation is due to differences in the individual geophone responses at these long periods. If the latter, the magnitudes of the changes suggest that the differences in the geophone responses are less than about 30%. Such response differences, if present, would not invalidate our major conclusions because they would appear to be only local perturbations rather than a uniform increase or decrease in the observed amplifications. Any systematic change in geophone response, such as the decrease in sensitivity with decreasing frequency, is taken into account when we take the spectral ratios relative to the same seismometers at the bedrock sites. The fact that all the bedrock sites show a similar response suggests that our reference sites are not plagued by an unusual geophone response.

We interpret the low signal-to-noise levels near 1.0 Hz as the primary cause of the mismatches between the spectral ratios of the Chi-Chi and local events at 1.0 Hz (Fig. 4) and of the wide variation in spectral ratios of the local events below 2.0 Hz (Fig. 4). The local earthquakes and blasts have large differences in amplification below 2.0 Hz, where the 4.5-Hz geophones have a low response. We considered removing the 0.7- to 2.0-Hz portion of the spectrum from the analysis, but retained the data because we felt that they provide upper bounds on the observed amplification levels despite the uncertainties introduced by the low signal-to-noise levels.

Results

The results (Figs. 4 and 6) show that weak ground motions in the 0.2- to 0.8-Hz frequency range (5- to 1.25-sec periods) are amplified by a factor of 8 or more at all sites over the central part of the Seattle basin (sites 1343–2645). The largest amplifications, factors of 12 to 16, occur over the east-central part of the basin at 0.3–0.6 Hz (3.33- to 1.67-sec periods). At lower frequencies (0.11 and 0.14 Hz; 9- and 7-sec periods, respectively), the basin causes amplifications of 3–6 (Fig. 6a). All of the basin sites show a trend of decreasing amplification with increasing frequency above 1 Hz (Fig. 4). At 7 Hz and above, the basin sites show less ground shaking than the reference sites (Fig. 6b). At bedrock sites (1002–1082, 2689–2852), the amplitudes are relatively low (Figs. 4 and 6) and the response is relatively flat across the spectrum (i.e., all the bedrock sites have nearly the same response as the two reference sites). The exception is station 2852, which is contaminated by high noise levels from 0.7 to 4 Hz (Figs. 3c, 4).

Our observations are consistent with previous site response studies in the 1- to 10-Hz range (Frankel *et al.*, 1999; Hartzell *et al.*, 2000; Frankel *et al.*, 2002), provided two differences between the studies are taken into account. First, the reference site in the previous studies is a “bedrock”

(“soft-rock”) site at Seward Park in the Seattle fault zone along the south edge of the Seattle basin (Fig. 1), or an idealized site with a velocity of 1 km/sec. The Seward Park reference site likely has a substantial thickness of sedimentary rock beneath it: it rests directly on sedimentary rocks equivalent to those in the lower part of the Seattle basin (Tertiary sandstone; $V_s = 433$ m/sec in upper 30 m [Williams *et al.*, 1999]), and basin sediments may lie beneath the south-dipping Seattle thrust fault under the reference sites (Johnson *et al.*, 1994; Pratt *et al.*, 1997; Brocher *et al.*, 2001a). Our site 5210, which is in a similar geologic setting to Seward Park (Fig. 1), shows amplification of about 1.5 in the 1- to 10-Hz range relative to our Olympic Mountains reference sites (Fig. 4). We thus expect site response estimates based on a Seward Park reference site to show amplitudes about 30% smaller than our estimates based on the Olympic Mountains reference sites. The Seward Park site shows a site response near 1 when compared to the idealized site with a velocity of 1 km/sec (Frankel *et al.*, 1999), suggesting that use of the idealized site is similarly underestimating the site response relative to our Olympic Mountain reference sites. The second difference is that the instruments in the previous studies were sited on a variety of surface deposits with large variations in shallow velocity (Williams *et al.*, 1999), in part to study areas known to have low-velocity surface deposits or strong shaking in earlier earthquakes. In contrast, we avoided siting our instruments on anomalous surface deposits such as artificial fill and Holocene river deposits.

For stiff-soil sites like those on which most of our instruments are sited, site response estimates using the Seward Park reference site indeed show amplifications of 1–3 near 1 Hz, generally decreasing to less than 1 for frequencies above 6 Hz (Frankel *et al.*, 1999; Hartzell *et al.*, 2000; Frankel *et al.*, 2002). Based on the previous discussion of the relative differences between reference sites, the amplification determined in previous studies is consistent with our local events being amplified by factors of 2–4 at 1.0 Hz and decreasing to an amplification of less than 1 above 7 Hz (Figs. 4, 6). Sites on soft fill and in West Seattle (an area of high amplification), for which we do not have comparable recordings, show amplifications of up to 10 relative to the Seward Park reference site and a steady decrease in amplitude at higher frequencies (Frankel *et al.*, 1999; Hartzell *et al.*, 2000; Frankel *et al.*, 2002). The amplifications in previous site response estimates thus are consistent with our results, and the shapes of the spectral ratio curves obtained over the Seattle basin show a decrease with increasing frequency that is similar to what we observe.

The amplification we observe for the Chi-Chi *S*-wave recordings changes with arrival time. To demonstrate this effect, we computed the spectral ratios in 30-sec time windows in the beginning, center, and end of our 100-sec analysis window (Fig. 7). At bedrock sites where the amplitudes are low, the 0- to 30-sec, 35- to 65-sec, and 70- to 100-sec portions of our original 100-sec time window all show simi-

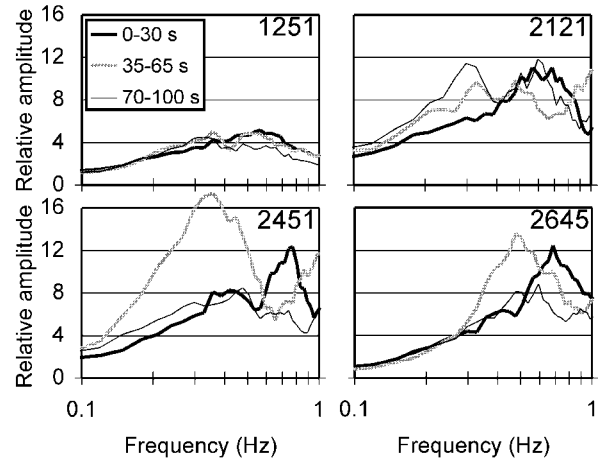


Figure 7. Spectral amplitudes at stations 1251, 2121, 2451, and 2645 showing the change in frequency and amplitude with time. The spectral amplitudes are from the 0- to 30-sec, 35- to 65-sec, and 70- to 100-sec portions of our 100-sec analysis window (Fig. 2). At sites with low amplitudes (e.g., 1251), the three time windows show a similar response. At sites with high amplitudes, arrivals in the first 30 sec are characterized by maximum amplitudes near 12 at frequencies of 0.5–0.8 Hz, whereas arrivals in the 35- to 65-sec time window have maximum amplitudes of 16 at lower frequencies (0.3–0.5 Hz). The 70- to 100-sec time window has variable amplitudes and frequencies across the array.

lar amplifications (e.g., site 1251 in Fig. 7). At basin sites where the amplitudes are large, the three windows have different responses. The first window has maximum amplifications of 10–12 with the peak at 0.5–0.8 Hz, the center time window shows amplifications as high as 16 with the peak at 0.3–0.5 Hz, and the last time window shows a response with wide variations but generally lower amplitudes than the first two windows. This change in amplification and frequency at later arrival times suggests that different mechanisms influence the earlier (0- to 30-sec) versus later (35- to 65-sec) amplification.

Interpretation

The *S*-wave arrivals from the Chi-Chi event that pass through the Seattle basin could be amplified by four distinct causes: (1) low-impedance sedimentary strata at the top of the basin will cause an amplitude increase and resonances (Shearer and Orcutt, 1987), (2) the Seattle basin or deeper structures may cause focusing (e.g., Aki and Larner, 1970), (3) reflections from the sides of the Seattle basin could constructively interfere with the direct arrivals, and (4) surface waves within the basin could have large amplitudes and long durations (Frankel and Stephenson, 2000; Frankel, 1994). The first of these effects is 1D, dependent only on the material directly below the instrument. The other effects are 3D in that they depend on the surrounding basin and other struc-

tures. We cannot accurately discern the relative sizes of these effects without detailed information about the shallow layers beneath the sites (e.g., from boreholes) and about the deep structure, but we can carry out several simple modeling exercises to estimate the relative sizes of at least some of these effects. The results show that the 1D effects could cause most of the amplification of the initial *S*-wave arrivals, but 3D effects are significant and may be the main cause of amplification at later arrival times.

To estimate the magnitude of the 1D resonance and impedance effects, we used a Thomson–Haskell method (Aki and Richards, 1980) to model waves propagating vertically through a stack of flat, homogeneous sediment layers above bedrock (Fig. 8a,b). As discussed in other studies (Shearer and Orcutt, 1987), individual layers introduce resonance peaks with amplitudes controlled by the impedance of the layers and with the frequency of the first, largest resonance peak determined by the travel time through the layer: $f = 1/(4T)$; f = frequency; T = one-way travel time.

As our models illustrate, thin, shallow, unconsolidated layers cause large resonance peaks at high frequencies because of their low impedance and small travel time through the layer, whereas the better consolidated, deeper layers produce smaller resonance peaks at lower frequencies (Fig. 8a). In particular, an interface at 1.9-sec one-way travel time (e.g., 2.5-km depth overlain by material with a velocity of 1300 m/sec) causes resonance at 0.15 Hz (6.67-sec period). This simple calculation indicates that resonance peaks on our 0.15- to 10-Hz spectrum most likely arise from layers within the upper half (<2.5-km depth) of the Seattle basin below our profile. Amplitude is largely unaffected by a layer at frequencies well below the first resonance peak, where the layer is thin in comparison to the wavelength (Fig. 8a).

In the case of the Seattle basin beneath our sites, modeling shows that the largest amplifications we observe in the initial arrivals (0–30 sec) could arise in a large part from 1D effects caused by the unconsolidated deposits that form the upper 450–550 m of the basin (Jones, 1996). Where measured, unconsolidated deposits in the upper 30 m in the Seattle area have average *S*-wave velocities of 150–680 m/sec (Williams *et al.*, 1999, 2000) and densities in the 1.6- to 2.4-gm/cm³ range (Galster and Laprade, 1991). These same glacial deposits extend across much of the Puget Lowland (Jones, 1996; Booth, 1994). We modeled a variety of thin-layer stacks to simulate the unconsolidated strata in the upper part of the basin, although these models are largely unconstrained because there is little information on the velocities of the unconsolidated strata directly beneath our stations. Our best match with the observed data was obtained by modeling the unconsolidated deposits as a 130-m-thick layer with an *S*-wave velocity of 500 m/sec underlain by a 180-m-thick layer with a velocity of 1000 m/sec. With these parameters, the largest resonance peak occurs at about 0.7 Hz and has an amplitude of more than 5 (Fig. 8b), similar in frequency to the largest resonance peaks we observe in the initial 30 sec of the *S*-wave arrivals (Fig. 7), but with only

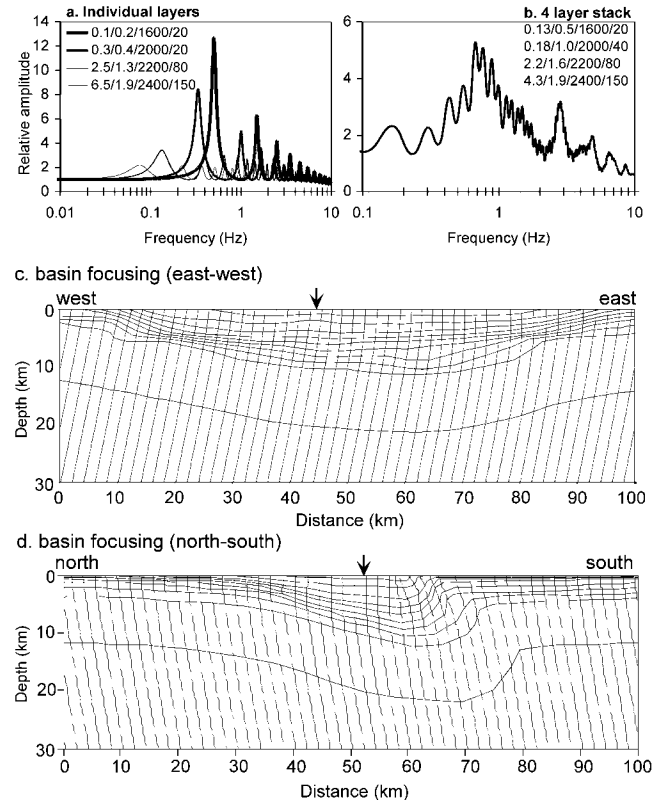


Figure 8. Models of site amplification over single layers (a), over a four-layer model of the Seattle basin (b), and models of focusing within the Seattle basin (c). The individual layers overlie a half space of Crescent Formation with an *S*-wave velocity (V_s) of 3.5 km/sec and a density (ρ) of 2900 kg/m³; for each layer the numbers list the thickness (km)/*S*-wave velocity (km/sec)/density (kg/m³)/attenuation factor (Q). (a) Model showing that shallow layers have resonance peaks with larger amplitude and higher frequency than those from the deep layers. (b) Model showing the response of a four-layer Seattle basin (layer parameters listed). (c) Raytrace model in east–west direction along the 1999 SHIPS profile. The velocity model is from the tomographic analysis of 1999 SHIPS and other data (Snelson *et al.*, 2000; Fig. 5, bottom). (d) Raytrace model in a north–south direction perpendicular to the 1999 SHIPS profile, using a model based on the refraction analysis of the 1998 SHIPS profile (Molzer *et al.*, 1999; ten Brink *et al.*, 2002). Arrows in panels c and d show the locations where the profiles cross. There is a relatively small focusing effect (5%–10%) in the east–west direction because the basin is relatively flat, but in the north–south direction the steep south edge bends rays into the basin.

about half the amplitude. Larger amplitudes are possible if the shallow deposits beneath our stations have lower velocities, but average velocities through the upper 100 m of these glacial tills would have to be unrealistically low (<200 m/sec) to match the observed 10- to 12-fold amplification with resonance and impedance effects alone. These models

thus show that 1D effects could cause a four- to sixfold amplification at some frequencies, requiring that 3D effects double or triple the amplitudes of these initial arrivals (0–30 sec) to reproduce the observed spectral ratios. Later arrivals (35–65 sec) have larger amplifications that require a greater influence from 3D effects, as observed elsewhere (e.g., Olsen, 2000).

Our 1D resonance models indicate that anelastic attenuation in the shallow sediments causes a substantial decrease in amplitude at higher frequencies. Amplitudes on the models drop below 1 (the input signal level) near 10 Hz (Fig. 8a,b). Models with high Q values (not shown) show a dramatically smaller decrease in amplitude at frequencies above 1 Hz. Thus, the decrease in amplitude at higher frequencies observed during the local events (Fig. 4) could be due largely to attenuation within the shallow layers.

Focusing by refraction of seismic waves into the low-velocity Seattle basin could increase amplitudes within the basin at the expense of amplitudes along its edges (e.g., Aki and Larner, 1970; Gao *et al.*, 1996; Davis *et al.*, 2000). To estimate the magnitude of the focusing effect in the Seattle basin for the specific case of the Chi-Chi earthquake, we traced rays upward through basin models derived from analyses of the SHIPS and other data (Molzer *et al.*, 1999; Snelson *et al.*, 2000; ten Brink *et al.*, 2002). Results show that focusing in the east–west direction likely has a minor effect on amplitudes ($\sim 10\%$ or less) because the basin is relatively flat in this direction (Fig. 8c).

There are two sources of focusing that could be significant. Focusing in a north–south direction is greater than in the east–west direction because the basin edges are steeper, particularly along the Seattle fault, where the velocity gradient is nearly vertical or there is a velocity inversion (Fig. 8d) (Brocher *et al.*, 2001a; ten Brink *et al.*, 2002). Our models show a substantial bending of rays toward the center of the basin, but the effect is highly dependent upon the complex, inadequately resolved velocity structure near the Seattle fault. This focusing effect also should be frequency dependent. At high frequencies the individual arrivals will be of short duration, and the focusing effect would cause localized areas of amplification and deamplification as waves constructively or destructively interfere. At low frequencies the arrivals will constructively interfere if the travel-time differences along the various ray paths are less than about one-fourth of the wavelength. For time delays that are 30% of the 1.5- to 2.2-sec one-way travel time through the basin (Johnson *et al.*, 1994; Pratt *et al.*, 1997), waves at frequencies below 0.56 Hz (1.8-sec period or greater) could have increased amplitudes across much of the basin due to focusing.

The other potential sources of focusing are deep sources such as the lower crust or upper mantle (e.g., Mori and Frankel, 1992), but again there is little information available to estimate the size of the focusing effect from these deep sources. Brocher *et al.* (in press) argued that a low-velocity upper mantle underlies the Puget Lowland, and Zhao *et al.*

(2001) saw tomographic evidence for lower velocities in the mantle east of Vancouver Island. The suggested mechanism for forming the low-velocity mantle is hydration (serpentinization) from water released by the subducted oceanic crust. If such a low-velocity zone is related to the development of the forearc, this effect would cause focusing largely in an east–west direction, but not along strike. A low-velocity mantle thus would focus waves toward the center of the Lowland, as we observe.

Like focusing, reflections from the sides of the basin could amplify low-frequency arrivals across large parts of the basin, but high-frequency waves are unlikely to constructively interfere except in localized areas. Reflections from sharp edges of the basin, such as the Seattle fault on its south edge or the Southern Whidbey Island fault zone on the northwest edge (Fig. 1), could constructively interfere with the direct arrivals to increase the amplitudes by as much as the reflection coefficient across these boundaries. For the Seattle basin, this reflection coefficient could be as large as 40%, but is likely lower. For example, the reflection coefficient would be 38% if we assume bedrock with a density of 2.9 g/cm³ and velocity of 3.5 km/sec is juxtaposed against basin fill with a density of 2.4 g/cm³ and velocity of 1.9 km/sec. There would be a large travel-time difference between a direct arrival and one reflected from the basin edge 10 km from our profile, however, so we expect constructive interference over broad regions of the basin to occur only at low frequencies where the long wavelengths are in phase over a larger area.

We interpret surface waves to be a major contributor to the longer durations and larger amplitudes we observe over the Seattle basin, and they provide a ready explanation for the change in amplification with time. Numerous observations, and modeling studies of ground shaking in sediment-filled valleys, show that surface waves originating from mode conversion at basin edges are trapped in the shallow deposits (Bard and Bouchon, 1980; Liu and Heaton, 1984; Vidale and Helmberger, 1988; Frankel and Vidale, 1992; Sánchez-Sesma *et al.*, 1993; Frankel, 1994; Sánchez-Sesma and Luzón, 1995; Olsen and Archuleta, 1996; Olsen, 2000). These surface waves are often responsible for the largest amplitudes observed at basin stations and are responsible for long durations of shaking.

Frankel *et al.* (2002) and Frankel and Stephenson (2000) examined the specific case of amplification by surface waves within the Seattle basin. They showed large-amplitude, late arrivals from the Nisqually earthquake at sites located on the Seattle basin. These late arrivals have the largest amplitudes of any arrivals at the basin sites, and they have long durations. Frankel *et al.* (2002) interpreted these arrivals as basin surface waves because of the relatively low group velocity (~ 2 km/sec) and the long durations. Observations of other earthquakes have shown a large-amplitude, dispersive phase arriving after the S wave at a site on the Seattle basin (Frankel and Stephenson, 2000). Modeling suggests these surface waves are higher order Rayleigh

waves produced primarily within the upper 2 km at the south edge of the Seattle basin (Frankel and Stephenson, 2000). On the models, the surface waves are trapped within the shallow sediments and become concentrated near the center of the basin where the shallow sediments thin to the north.

The arrivals on our seismograms at 40–100 sec (Fig. 2) are consistent with surface waves coming from multiple directions: they are evident on the vertical component, and they are incoherent across our array (because of our large station spacing). The vertical component recordings show significant arrivals beginning 20 sec after the initial *S*-wave arrival, suggesting surface waves and other scattered arrivals become significant at about this time. The duration of shaking at basin sites relative to bedrock sites is remarkable (Figs. 2 and 3a), suggesting that the long duration of shaking contributes significantly to the large spectral amplifications we compute in our 100-sec analysis window. These long-duration waves dominate the seismograms, suggesting they are also the dominant cause of the 16-fold amplification we see at some sites in the 35- to 65-sec analysis window (Fig. 7).

The layers trapping the surface waves within the Seattle basin are most likely the unconsolidated deposits forming the top 450–550 m beneath our profile (Jones, 1996). Frankel and Stephenson (2000) found that long-period surface waves were efficiently trapped within a low-velocity layer in the upper 800 m of their model. The strong 0.4- to 0.8-Hz resonances that we observe during the early part of the *S*-wave arrivals indicate that strong reflectors, and therefore large velocity increases that can trap surface waves, lie within the upper 450 m. The characteristic frequency of about 0.3–0.5 Hz for the surface waves we observe could be due to the detailed mechanical properties and geometry of the surface layer, the geometry of the basin edges where mode conversion is occurring, or attenuation of waves at higher frequencies. Joyner (2000) suggested that body waves dominate the ground motions at periods of 0.33 Hz and higher (<3-sec periods) because anelastic attenuation reduces the surface wave amplitude. At frequencies below 0.33 Hz (>3-sec periods), Joyner (2000) argued that the surface waves become dominant. This explanation appears to be consistent with our observations.

Discussion

The amplification we observe for the Chi-Chi arrivals is surprisingly large, but it is important to note that these amplifications pertain only to the weak ground motions we observe. During strong shaking ($>0.2g$), the amplification may be less because of nonlinear soil response like that observed within the Seattle basin during the recent Nisqually earthquake (Frankel *et al.*, 2002), in other basins (Chin and Aki, 1991; Hartzell, 1998; Field *et al.*, 1997, 1998) and predicted from modeling of soils (Yu *et al.*, 1993).

Frankel *et al.* (2002) compared weak and strong ground motions during the 2001 *M* 6.8 Nisqually earthquake and an M_L 3.4 aftershock. Weak ground motions during the after-

shock show amplifications of 1.7–4.0 in the frequency band centered on 3.3 Hz, but the mainshock shows amplifications of only 1.0–1.4 at these same sites. At 5 Hz the aftershock showed amplifications of 1.5–4.0 at soft-soil sites but little amplification during the mainshock. Amplifications during the Nisqually mainshock were apparently reduced by nonlinear soil response, despite the relatively modest peak acceleration of 0.15*g* to 0.22*g*.

We cannot conclude from analysis of the Nisqually earthquake, however, that nonlinear soil response will significantly decrease the amplification we observe over the Seattle basin at accelerations above 0.2*g*. Frankel *et al.* (2002) were seeing the nonlinear response only at soft-soil sites. At stiff-soil sites, like those on which most of our sites are located, they observed little difference in amplification between the mainshock and aftershock at accelerations of up to 0.22*g*. The upper limit of linear response is unknown for stiff-soil sites in the Puget Lowland. Thus, our results indicate that stiff-soil sites located over the Seattle basin will see substantial amplification due to the basin, perhaps at accelerations significantly higher than 0.2*g*.

Sedimentary basins beneath the Puget Lowland are capped by a layer of relatively stiff glacial deposits that likely have a similar surface velocity across the basin (Booth, 1994). These glacial deposits may dominate the site response effects at most frequencies through 1D effects and surface waves, resulting in a weak correlation between site amplification and overall basin thickness. The fact that our largest amplifications occur over the center and east parts of the Seattle basin could be due more to focusing and to the convergence of surface waves (e.g., Olsen and Archuleta, 1996; Frankel and Stephenson, 2000) than to differences in the velocity of the shallowest strata across the basin. Figure 7 shows a similar response at basin sites for the 0- to 30-sec arrivals, which we interpret as being dominated by body waves. During the 35- to 65-sec time window, which we interpret as being dominated by surface waves, Figure 7 shows much larger amplitudes near the center and east side of the basin. If this pattern holds for all events, the body waves amplified in the shallow sediments (Joyner, 2000) will show a stronger correlation with artificial fill or Holocene sediments in river valleys (Frankel *et al.*, 2002) than with deeper basin morphology. The glacial tills also cap the nearby Everett and Tacoma basins and extend beyond the basins, suggesting that other areas of the Puget Lowland could see substantial seismic-wave amplification by the glacial tills.

This study also illustrates the potential role of the 1D and 3D basin geometry on ground shaking. Initial body-wave arrivals appear to be dominated by amplification through 1D effects (impedance changes, resonance), which can amplify the direct arrivals by factors of 4 to 6 at basin sites for some frequencies. 3D effects (focusing, scattering, surface waves) apparently increase the amplitudes of the initial arrivals by only a factor of 2–3, implying that the 1D effects have nearly twice the influence as 3D effects on the

direct arrivals from below the Seattle basin. Later arrivals, on the other hand, appear to be dominated by the basin surface waves beginning 20–40 sec after the initial shear-wave arrivals. The 1D effects and the surface waves both appear to arise within the unconsolidated deposits forming the upper portions of the basin. Our results thus emphasize the need to better map the velocity structure of these shallow deposits if we are to understand the influence sedimentary basins have on ground shaking in the Puget Lowland.

Acknowledgments

We thank the 40 volunteers who deployed the SHIPS seismometers. The Incorporated Research Institutes for Seismology (IRIS) provided the seismometers and technical support. Tom Burdette, Tom Yelin, Karen Meagher, and Bob Norris of the USGS and personnel from UTEP, UW, and OSU contributed immensely to the SHIPS project. Charles Mueller of the USGS in Golden, Colorado, provided the 1D modeling software (RATTLE), and Jim Luetgert of the USGS in Menlo Park, California, provided the 2D modeling software (MacRay). Reviews by Art Frankel, Susan Hough, Ken Campbell, and an anonymous reviewer resulted in many improvements of the manuscript.

References

- Aki, K., and K. L. Larner (1970). Surface motion of a layered medium having an irregular interface due to incident SH waves, *J. Geophys. Res.* **75**, 933–954.
- Aki, K., and P. G. Richards (1980). *Quantitative Seismology: Theory and Methods*, W. H. Freeman, New York.
- Atkinson, G. M. (1995). Attenuation and source parameters of earthquakes in the Cascadia region, *Bull. Seism. Soc. Am.* **85**, 1327–1342.
- Atwater, B. F. (1996). Coastal evidence for great earthquakes in western Washington, in *Assessing Earthquake Hazards and Reducing Risk in the Pacific Northwest*, A. M. Rogers, W. J. Kockelman, G. R. Priest, and T. M. Walsh (Editors), *U.S. Geol. Surv. Profess. Pap. 1560*, 77–90.
- Bard, P. Y., and M. Bouchon (1980). The seismic response of sediment-filled valleys. I. The case of incident SH-waves, *Bull. Seism. Soc. Am.* **70**, 1263–1286.
- Booth, D. B. (1994). Glaciofluvial infilling and scour of the Puget Lowland, Washington, during ice-sheet glaciation, *Geology* **22**, 695–698.
- Brocher, T. M., T. Parsons, R. J. Blakely, N. I. Christensen, M. A. Fisher, R. E. Wells, and SHIPS working group (2001a). Upper crustal structure in Puget Lowland, Washington: results from the 1998 Seismic Hazards Investigation in Puget Sound, *J. Geophys. Res.* **106**, 13,541–13,564.
- Brocher, T. M., T. Parsons, A. M. Tréhu, C. M. Snelson, and M. A. Fisher (2003). Seismic evidence for widespread serpentinized forearc upper mantle along the Cascadia Margin, *Geology* (in press).
- Brocher, T. M., T. L. Pratt, K. C. Creager, R. S. Crosson, W. P. Steele, C. S. Weaver, A. D. Frankel, A. M. Tréhu, C. M. Snelson, K. C. Miller, S. H. Harder, and U. S. ten Brink (2000a). Urban seismic experiments investigate Seattle fault and basin, *EOS* **81**, 545–552.
- Brocher, T. M., T. L. Pratt, and Dry SHIPS Working Group (2001b). Dry SHIPS recordings of the Chi-Chi earthquake, Seattle, Washington, *Bull. Seism. Soc. Am.* **96**, 1395.
- Brocher, T. M., T. L. Pratt, K. C. Miller, A. M. Tréhu, C. M. Snelson, C. S. Weaver, K. S. Creager, R. S. Crosson, U. S. ten Brink, M. G. Alvarez, S. H. Harder, and I. Asudeh (2000b). *Report for Explosion and Earthquake Data Acquired in the 1999 Seismic Hazard Investigation of Puget Sound (SHIPS)*, Washington, *U.S. Geol. Surv. Open-File Report 00-318*.
- Bucknam, R. C., E. Hemphill-Haley, and E. B. Leopold (1992). Abrupt uplift within the past 1700 years at southern Puget Sound, Washington, *Science* **258**, 1611–1614.
- Carver, D. L., K. W. King, R. A. Williams, and D. M. Worley (1998). Earthquake ground-response studies in west and south Seattle, Washington, in *Assessing Earthquake Hazards and Reducing Risk in the Pacific Northwest*, A. M. Rogers, W. J. Kockelman, G. R. Priest, and T. M. Walsh (Editors), *U.S. Geol. Surv. Profess. Pap. 1560*, Vol. 2, 345–354.
- Chin, B.-H., and K. Aki (1991). Simultaneous study of the source, path, and site effects on strong ground motion during the 1989 Loma Prieta earthquake: a preliminary result on pervasive nonlinear site effects, *Bull. Seism. Soc. Am.* **81**, 1859–1884.
- Davis, P. M., J. L. Rubinstein, K. H. Liu, S. S. Gao, and L. Knopoff (2000). Northridge earthquake damage caused by geologic focusing of seismic waves, *Science* **289**, 1746–1750.
- Field, E. H., P. A. Johnson, I. A. Beresnev, and Y. Zeng (1997). Nonlinear ground-motion amplification by sediments during the 1994 Northridge earthquake, *Nature* **390**, 599–602.
- Field, E. H., Y. Zeng, P. A. Johnson, and I. A. Beresnev (1998). Pervasive nonlinear sediment response during the 1994 Northridge earthquake: observations and finite-source simulations, *J. Geophys. Res.* **103**, 26,869–26,884.
- Frankel, A. (1994). Dense array recordings in the San Bernardino Valley of Landers–Big-Bear aftershocks: basin surface waves, Moho reflections, and three-dimensional simulations, *Bull. Seism. Soc. Am.* **84**, 613–624.
- Frankel, A., and W. Stephenson (2000). Three-dimensional simulations of ground motions in the Seattle region for earthquakes on the Seattle fault zone, *Bull. Seism. Soc. Am.* **90**, 1251–1267.
- Frankel, A., and J. Vidale (1992). A three-dimensional simulation of seismic waves in the Santa Clara Valley, California, from a Loma Prieta aftershock, *Bull. Seism. Soc. Am.* **82**, 2045–2074.
- Frankel, A., D. Carver, E. Cranswick, M. Meremonte, T. Bice, and D. Overturf (1999). Site response for Seattle and source parameters of earthquakes in the Puget Sound region, *Bull. Seism. Soc. Am.* **89**, 468–483.
- Frankel, A. D., D. L. Carver, and R. A. Williams (2002). Nonlinear and linear site response and basin effects in Seattle for the M6.8 Nisqually, Washington, earthquake, *Bull. Seism. Soc. Am.* **92**, 2090–2109.
- Galster, R. W., and W. T. Laprade (1991). Geology of Seattle, Washington, United States of America, *Bull. Assoc. Eng. Geol.* **28**, 235–302.
- Gao, S. H., P. M. Liu, P. M. Davis, and L. Knopoff (1996). Localized amplification of seismic waves and correlation with damage due to the Northridge earthquake: evidence for focusing in Santa Monica, *Bull. Seism. Soc. Am.* **86**, S209–S230.
- Hartzell, S. (1998). Variability in nonlinear sediment response during the 1994 Northridge, California, earthquake, *Bull. Seism. Soc. Am.* **88**, 1426–1437.
- Hartzell, S., D. Carver, E. Cranswick, and A. Frankel (2000). Variability of site response in Seattle, Washington, *Bull. Seism. Soc. Am.* **90**, 1237–1250.
- Hartzell, S., A. Leeds, A. Frankel, R. A. Williams, J. Odum, W. Stephenson, and W. Silva (2002). Simulation of broadband ground motion including nonlinear soil effects for a magnitude 6.5 earthquake on the Seattle fault, Seattle, Washington, *Bull. Seism. Soc. Am.* **92**, 831–853.
- Ihnen, S. M., and D. M. Hadley (1986). Prediction of strong ground motion in the Puget Sound region: the 1965 Seattle earthquake, *Bull. Seism. Soc. Am.* **76**, 905–922.
- Johnson, S. Y., C. J. Potter, and J. M. Armentrout (1994). Origin and evolution of the Seattle fault and Seattle basin, Washington, *Geology* **22**, 71–74.
- Jones, M. A. (1996). Thickness of unconsolidated deposits in the Puget Sound Lowland, Washington and British Columbia, *U.S. Geol. Surv. Water Resour. Invest. Report 94-4133*.
- Joyner, W. B. (2000). Strong motion from surface waves in deep sedimentary basins, *Bull. Seism. Soc. Am.* **90**, S95–S112.

- Langston, C. A., and J.-J. Lee (1983). Effect of structure geometry on strong ground motions: the Duwamish River Valley, Seattle, Washington, *Bull. Seism. Soc. Am.* **73**, 1851–1863.
- Liu, H.-L., and T. Heaton (1984). Array analysis of the ground velocities and accelerations from the 1971 San Fernando, California, earthquake, *Bull. Seism. Soc. Am.* **74**, 1951–1968.
- Molzer, P. C., U. S. ten Brink, M. A. Fisher, T. M. Brocher, K. C. Creager, and R. S. Crosson (1999). Seismic structure of Seattle fault, Seattle basin, and Kingston arch, Washington, *EOS* **80**, F762.
- Mori, J., and A. Frankel (1992). Correlation of *P* wave amplitudes and travel time residuals for teleseisms recorded on the southern California seismic network, *J. Geophys. Res.* **97**, 6661–6674.
- Olsen, K. B. (2000). Site amplification in the Los Angeles basin from three-dimensional modeling of ground motion, *Bull. Seism. Soc. Am.* **90**, S77–S94.
- Olsen, K. B., and R. J. Archuleta (1996). Three-dimensional simulation of earthquakes on the Los Angeles fault system, *Bull. Seism. Soc. Am.* **86**, 575–596.
- Pratt, T. L., S. Johnson, C. Potter, W. Stephenson, and C. Finn (1997). Seismic reflection images beneath Puget Sound, western Washington State: the Puget lowland thrust sheet hypothesis, *J. Geophys. Res.* **102**, 27,469–27,489.
- Sánchez-Sesma, F. J., and F. Luzón (1995). Seismic response of three-dimensional alluvial valleys for incident *P*, *S*, and Rayleigh waves, *Bull. Seism. Soc. Am.* **85**, 269–284.
- Sánchez-Sesma, F. J., S. Chávez-Pérez, M. Suarez, M. A. Bravo, and L. E. Pérez-Rocha (1988). On the seismic response of the Valley of Mexico, *Earthquake Spec.* **4**, 569–589.
- Sánchez-Sesma, F. J., L. E. Pérez-Rocha, and E. Reinoso (1993). Ground motion in Mexico City during the April 25, 1989, Guerrero earthquake, *Tectonophysics* **218**, 127–140.
- Shearer, P. M., and J. A. Orcutt (1987). Surface and near-surface effects on seismic waves: theory and borehole seismometer results, *Bull. Seism. Soc. Am.* **77**, 1168–1196.
- Shin, T. C., K. W. Kuo, W. H. K. Lee, T. L. Teng, and Y. B. Tsai (2000). A preliminary report on the 1999 Chi-Chi (Taiwan) earthquake, *Seism. Res. Lett.* **71**, 24–30.
- Snelson, C. M., K. C. Miller, T. M. Brocher, T. L. Pratt, A. M. Tréhu, and C. S. Weaver (2000). Results of the 1999 Dry SHIPS (Seismic Hazard Investigations of Puget Sound) Seismic Experiment in western Washington, *EOS* **81**, F871.
- ten Brink U. S., P. C. Molzer, M. A. Fisher, R. J. Blakely, R. C. Bucknam, T. Parsons, R. S. Crosson, and K. C. Creager (2002). Subsurface geometry and evolution of the Seattle fault zone and the Seattle basin, Washington, *Bull. Seism. Soc. Am.* **92**, 1737–1753.
- Vidale, J. E., and D. V. Helmberger (1988). Elastic finite-difference modeling of the 1971 San Fernando, California earthquake, *Bull. Seism. Soc. Am.* **78**, 122–141.
- Van Wagoner, T. M., R. S. Crosson, K. C. Creager, G. Medema, L. Preston, N. P. Symons, and T. M. Brocher (2002). Crustal structure and re-located earthquakes in the Puget Lowland, Washington, from high resolution seismic tomography, *J. Geophys. Res.* **107**, no. B12, 22-1–22-23.
- Wald, D. J., and R. W. Graves (1998). The seismic response of the Los Angeles Basin, California, *Bull. Seism. Soc. Am.* **88**, 337–356.
- Williams, R. A., W. J. Stephenson, A. D. Frankel, and J. K. Odum (1999). Surface seismic measurements of near-surface *P*- and *S*-wave seismic velocities at earthquake recording stations, Seattle, Washington, *Earthquake Spec.* **15**, 565–584.
- Williams, R. A., W. J. Stephenson, A. D. Frankel, E. Cranswick, M. E. Meremonte, and J. K. Odum (2000). Correlation of 1- to 10-Hz earthquake resonances with surface measurements of *P*- and *S*-wave reflections and refractions in the upper 50 m, *Bull. Seism. Soc. Am.* **90**, 1323–1331.
- Yu, G., J. G. Anderson, and R. Siddharthan (1993). On the characteristics of nonlinear soil response, *Bull. Seism. Soc. Am.* **83**, 218–224.
- Zhao, D., K. Wang, G. C. Rogers, and S. M. Peacock (2001). Tomographic image of low *P* velocity anomalies above slab in northern Cascadia subduction zone, *Earth Planets Space* **53**, 285–293.
- U.S. Geological Survey
University of Washington
Seattle, Washington 98195
(T.L.P., C.S.W.)
- U.S. Geological Survey
345 Middlefield Road
Menlo Park, California 94025
(T.M.B.)
- Department of Geophysics
University of Washington
Seattle, Washington 98195
(K.C.C., R.S.C.)
- Department of Geological Sciences
University of Texas
El Paso, Texas 79968
(C.M.S., K.C.M.)
- College of Ocean and Atmospheric Sciences
Oregon State University
Corvallis, Oregon 97331
(A.M.T.)